International Journal of Fatigue 32 (2010) 621–626

Contents lists available at ScienceDirect

International Journal of Fatigue

journal homepage: www.elsevier.com/locate/ijfatigue

Effect of alumite surface treatments on long-life fatigue behavior of a cast aluminum in rotating bending

Yuki Nakamura [a,*], Tatsuo Sakai [a], Hideo Hirano [b], K.S. Ravi Chandran [c]

[a] College of Science and Engineering, Ritsumeikan University, 1-1-1 Nojihigashi, Kusatsu, Shiga 525 8577, Japan
[b] Home Appliances Company, Panasonic Co., Ltd., 2-3-1-2 Nojihigashi, Kusatsu, Shiga 525 8520, Japan
[c] Department of Metallurgical Engineering, The University of Utah, 135 South 1460 East Rm. 412, Salt Lake City, UT 84112, USA

ARTICLE INFO

Article history:
Received 7 January 2009
Received in revised form 18 August 2009
Accepted 5 October 2009
Available online 13 October 2009

Keywords:
Alumite treatment
Long-life fatigue
Aluminum alloy
Rotating bending
Fractography

ABSTRACT

Alumite treatment is one of surface treatments for aluminum alloy and it provides an oxide layer (Al_2O_3) on the surface by anodizing. The oxide layer is called "alumite" in Japanese industry. This method has been widely used for aluminum alloy because the alumite possesses characteristics such as high hardness, wear resistance, and electrical resistance. In order to examine the effect of alumite layer on the fatigue behavior, fatigue tests were carried out on aluminum alloy specimens with two different alumite treatments by means of a dual-spindle rotating bending fatigue testing machine. Tests were also conducted on untreated specimens for comparison. Fracture surfaces of all the failed specimens were examined in a scanning electronic microscope (SEM). Fatigue fracture mechanisms are discussed in the light of fractography and fracture mechanics.

As results of fatigue tests, significant deteriorations of the fatigue strength for alumite-treated specimens having each thickness of the alumite layer were observed in comparison with the results for untreated specimen in the short life regime. However, in long-life regime of $>10^7$, the fatigue strength of alumite-treated specimen having 3 μm alumite layer becomes a little higher than the results for untreated specimen.

1. Introduction

In recent years, some components of mechanical structures have been exposed in a long sequence of the cyclic loading such as gigacycle regime [1,2], and we have a new trend that replacement of the large-scale mechanical structures used in various applications is difficult from economic and environmental considerations. They may have to be used for longer times, sometimes, beyond their original design lives, to save resources, to reduce energy consumption in manufacturing and to reduce waste [3,4]. For example, if the design life of a mechanical product is doubled, the consumption of resources and energy as well as the generation of waste are also reduced proportionately. Accordingly, there can be synergistic multiple benefits that increase the sustainability in society [5,6].

In parallel, there are increasingly stringent requirements for the safety of machines and structures. Under these circumstances, fatigue behavior of structural materials in the very high cycle regime such as (10^9–10^{10}) cycles has become a priority in fatigue research [7,8]. Research in this area is increasing, as evidenced by some international conferences and publication of special issues in journals, in recent years [9–13].

Aluminum alloys have been widely used as structural materials due to their light weight, ease of recycling, optimum physical and mechanical properties as well as good surface characteristics [14–17]. However, researches on the long-life fatigue behavior of aluminum alloys are relatively few, compared to ferrous metals. In the conventional concept of the *S–N* fatigue curve, ferrous metals have been considered to show distinct fatigue limits, whereas non-ferrous metals have been considered to show no fatigue limit, with the curves decreasing continuously with an increase of the number of stress cycles to failure [18]. The question of whether this notion is still reasonable in the very high cycle regime is one of important questions to be resolved yet.

In this research, fatigue behavior of an aluminum alloy in the very high cycle regime has been investigated. The "alumite treatment", where an Al_2O_3 layer is formed on the surface of the aluminum alloy through anodizing, is often given to components due to the superior hardness, wear resistance, and electrical resistance of the layer.

In this study, three different sets of specimens of TF12B-T6 aluminum alloy were prepared for the evaluation of fatigue behavior. The first is the base alloy without alumite treatment, the second is the set of specimens with the alumite layer thickness of 3 μm and

* Corresponding author. Tel.: +81 77 561 2745; fax: +81 77 561 2665.
E-mail address: rm012034@ed.ritsumei.ac.jp (Y. Nakamura).

0142-1123/$ - see front matter © 2009 Elsevier Ltd. All rights reserved.
doi:10.1016/j.ijfatigue.2009.10.002

the third is another set of specimens with alumite layer thickness of 10 μm. Fatigue characteristics were studied experimentally in the ultra-long-life regime in rotating bending. Fatigue mechanisms were identified by fractography using SEM. The effects of alumite treatment on fatigue behavior and fracture mechanisms are discussed in the light of fractography and fracture mechanics.

2. Materials and experimental procedures

2.1. Materials

Material used in this study was a cast aluminum alloy, TF12B. Chemical composition of the alloy TF12B is given in Table 1. TF12B was solution treated at 495 °C for 2 h and aged at 175 °C for 4 h. The microstructure of the alloy was observed by means of an optical microscope. An example of the microscopic observations was shown in Fig. 1, where a distribution of Si rich eutectic particles that have been spheriodized through the addition of Sr, can be seen. Some of Si rich eutectic particles tend to appear along the grain boundaries, while the other Si rich eutectic particles appear inside the Al grains. The Al grain size is in a range of 20–50 μm. These Si rich eutectic particles were formed in the process of solidification and dispersed in the Al matrix. Mechanical properties of this alloy are given in Table 2.

The alumite treatment was performed in order to produce the Al_2O_3 layer on the specimen surface by anodizing, through the following process; Pretreatment to remove oil and fat on specimen surface was made by using acetone, after which the alumite treatment was carried out through anodizing in sulphuric electrolytic bath. Specimen surface was finally washed by hot water and dried by blowing air. By adjusting the anodizing time, thickness of the alumite layer was controlled. Specimens having two different thicknesses of alumite layers, viz., 3 μm and 10 μm, were prepared. It was very difficult to keep the uniform thickness of the alumite layer. Thus, the above values of the thickness have resulted as the average over the entire circumference of the cross section of the specimen.

Table 1
Chemical composition (wt.%).

Si	Cu	Mg	Fe	Ni	Cr	Mn	Sr	Ti	V	Al
10	4	0.6	0.2	0.2	0.06	0.01	0.01	0.01	0.01	Bal.

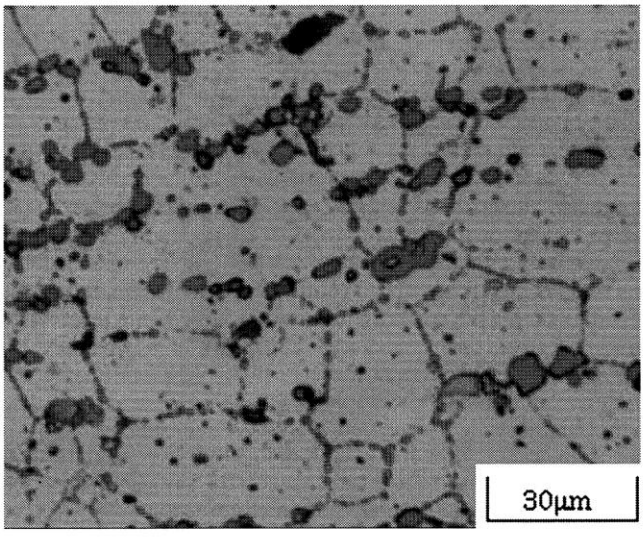

Fig. 1. Microstructure of TF12B-T6.

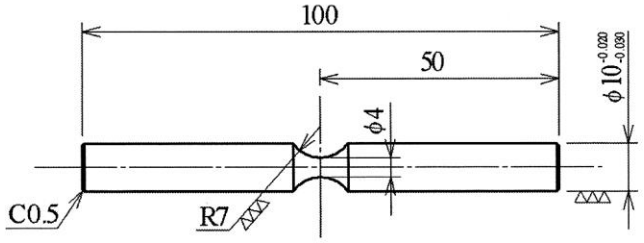

Fig. 2. Shape and dimensions of frtigue specimen.

2.2. Experimental procedures

The shape and dimensions of fatigue specimen are shown in Fig. 2. The diameter of the minimum cross-section is 4.0 mm and the stress concentration factor on the reduced cross sectional area is 1.08, as determined from Peterson's handbook [19].

In order to perform fatigue tests efficiently in very high cycle regime, the authors had developed a multi-type fatigue testing machine in rotating bending. The machine has two spindles driven by an electric motor via a flat belt, and each spindle has specimen grips at both ends [20,21]. Thus, one can perform fatigue tests of four specimens simultaneously by using this machine. Eccentricity of the specimens mounted to the specimen grips was kept within ±20 μm at the tip of each specimen. The rotating speed of the spindle is 3150 rpm. All the fatigue tests were conducted at room temperature and in laboratory environment. After fatigue tests, fracture surfaces of failed specimens were examined in a scanning electronic microscope (SEM).

3. Results and discussion

3.1. S–N characteristics

Fatigue test data obtained for the TF12B aluminum alloy of with and without the alumite treatments are given in Fig. 3. In each set of specimens, data points for failures due to surface-initiated cracks are shown by open symbols and failure due to interior-crack-initiations are shown by closed symbols. Data points with arrows attached indicate the run-outs. In the case of untreated specimens, surface-crack-initiations occurred at stress levels ≧175 MPa, whereas interior-crack-initiations occurred at stress levels <175 MPa. However, *S–N* curves for the respective failure modes were smoothly connected at the critical stress level causing the separation of the failure mode. Therefore, a smooth *S–N* curve is seen in the cycle range of $10^3 < N < 10^9$.

In the case of alumite-treated specimens having 3 μm alumite layer, the failure mode shifted from surface-initiated failures to interior-initiated failures at a stress amplitude level of about

Table 2
Mechanical properties.

Tensile strength (MPa)	0.2% yield stress (MPa)	Elongation (%)	Reduction of area (%)	Young's modulus (GPa)	Vickers hardness HV
407	355	4.7	8.0	78.8	148

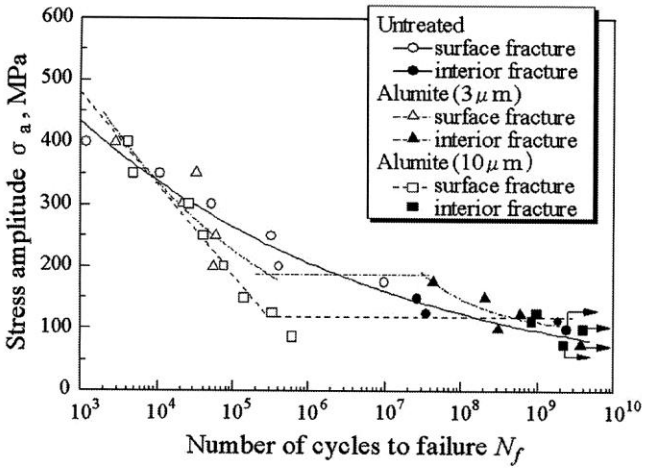

Fig. 3. *S–N* diagram for TF12B-T6 aluminum alloy, with and without alumite treatments.

200 MPa. The transition in the failure modes is relatively more distinct, compared to that of the untreated specimen. Therefore, it can be said that the fatigue behavior of 3 μm alumite-treated specimen shows duplex *S–N* characteristics, a behavior, often reported for the high strength steels [4,20,22]. Apparent fatigue limit for the surface-initiated failure was determined as the average value of the lowest stress level giving the surface-initiated failure and the highest stress level giving the interior-initiated failure. Thus, we have the value of 188 MPa and a horizontal chained line is indicated at this level in Fig. 3 for the sake of convenience. At stress levels <300 MPa, the fatigue strength of all the alumite-treated specimens is lower than that of the untreated specimen, as far as only the surface-initiated failure is concerned. At higher stress levels >300 MPa, difference of the fatigue strength is not clear due to a shortage of the experimental data.

For the specimen having 10 μm alumite layer, it is clear that a significant deterioration of the fatigue strength is observed, compared to all other surface conditions. Only two cases of interior-initiated failure were observed at 125 MPa and 112.5 MPa. The *S–N* curve for the interior-initiated failure may appear, if more number of fatigue tests were carried out in the very high cycle regime of $N_f > 10^9$. Horizontal portion of the dashed *S–N* curve was determined similar to the case of the chained *S–N* curve for 3 μm alumite layer specimens. Physical meaning of the horizontal portion of *S–N* curves for alumite-treated specimens in Fig. 3 is discussed from a viewpoint of fracture mechanics in the section of "Fracture Mechanics Analysis".

Finally, it should be noted that specimens sustain several thousand cycles even at the stress level near the ultimate tensile strength as reported by many researchers [18]. This aspect can be attributed to the fact that the stress acting at specimen surface changes instantaneously from tension to compression due to high speed revolution and, therefore, the fracture cannot occur at the moment of the maximum tension.

3.2. SEM observations

Fig. 4a shows the SEM image of the crack initiation site of an untreated specimen failed at 350 MPa with $N_f = 11{,}060$. No defect (porosity or inclusion) was found at the crack initiation site. Fig. 4b shows the crack initiation site of an untreated specimen failed at 150 MPa with $N_f = 267{,}95{,}930$. In this case, a cluster of pores was found at the crack initiation site. A concept of $\sqrt{area}$ proposed by Y. Murakami was accepted to evaluate the size of the

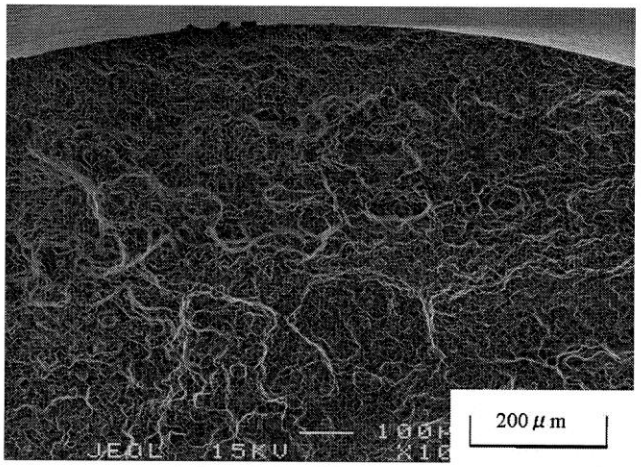

(a) Example at σ_a=350MPa, N_f=11,060

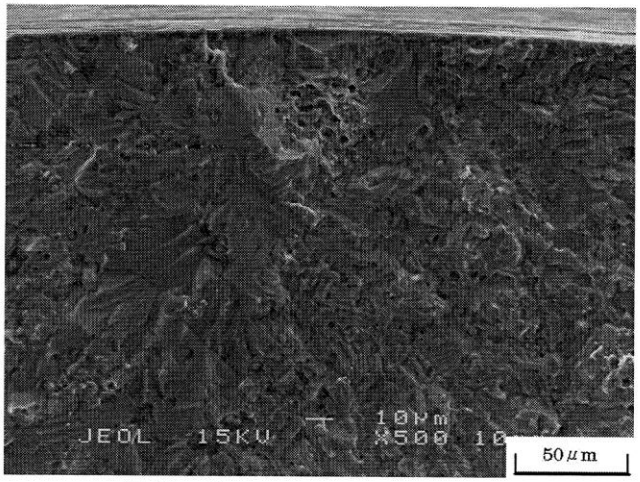

(b) Example at σ_a=150MPa, N_f=26,795,930

Fig. 4. Crack initiation sites in untreated specimens.

pores cluster and the numerical result measured in Fig. 4b was 54 μm. Detailed aspects such as distribution pattern of the pore size and the kind of the pore are still unsolved at the present stage of the study. However, it is noted that the above cluster of pores can play an important role in the fatigue crack initiation of this material.

A couple of examples of crack initiation sites in specimens with 3 μm alumite layer are shown in Fig. 5. Fig. 5a shows the crack initiation site of the specimen failed at 300 MPa with $N_f = 21{,}749$. The site of the origin of the dominant crack leading to the final failure corresponded to the thickest region of the alumite layer. Breakage of the alumite layer has happened in the process of the surface treatment, i.e., before the fatigue test as explained in the next paragraph. Thus, the breakage of the alumite lyer plays a role as the crack starter into the parent material. Fig. 5b shows the crack initiation site of the specimen failed at 100 MPa and $N_f = 3069{,}82{,}290$. A cluster of pores was seen beneath the specimen surface, quite similar to that in Fig. 4b, suggesting fatigue crack initiation from the pores. The value of $\sqrt{area}$ was also measured in Fig. 5b similar to the above example and we have the result of 141 μm in this case.

As mentioned above, the fatigue crack tends to initiate at the specimen surface having a thick alumite layer, but the crack tends to initiate at a porous area in subsurface in the case of specimen having a thin alumite layer. In order to check this point, notch root surface of the specimen having the alumite layer of 3 μm thick was examined in an SEM before the fatigue test. As shown in Fig. 6, a

number of micro-cracks were found in the alumite layer at the notch root. Initiation mechanism of these micro-cracks is not unsolved at the present stage of this study, but it is easily suggested that these cracks can be crack starters for the parent material in the sequence of cyclic loading.

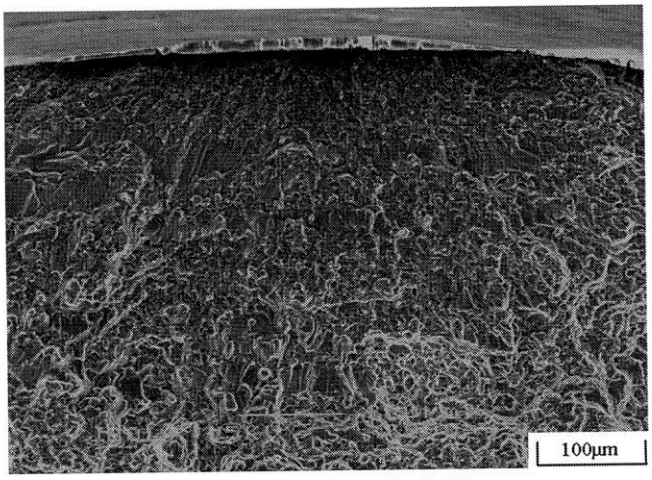

(a) Example at σ_a=300MPa, N_f=21,749

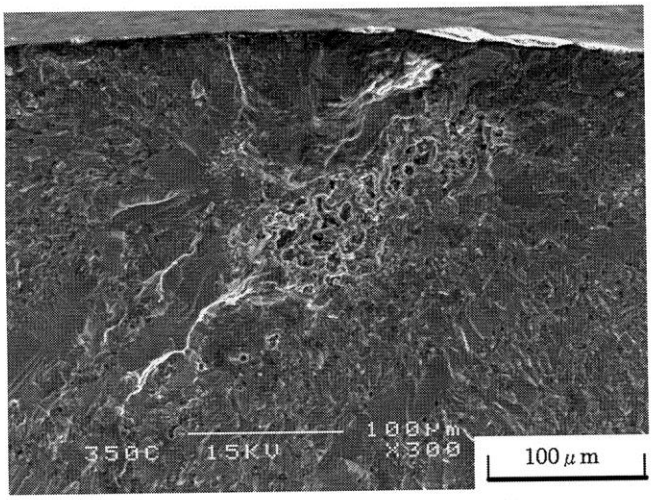

(b) Example at σ_a=100MPa, N_f=306,982,290

Fig. 5. Crack initiation sites in alumite (3 μm) specimens.

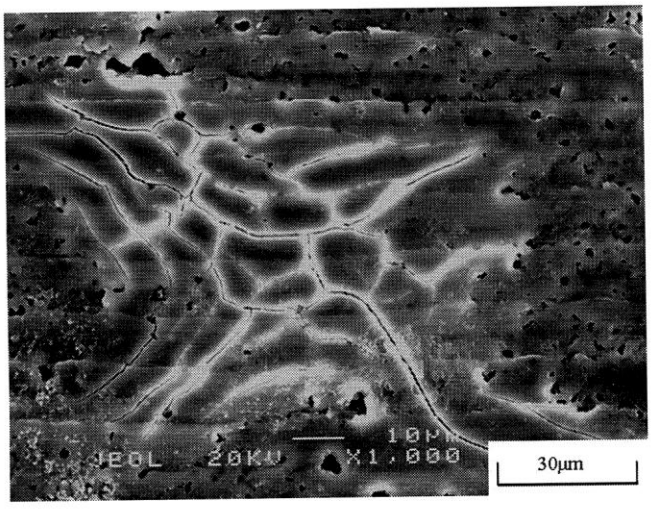

Fig. 6. Presence of micro-cracks at the notch root surface of alumite (3 μm) specimen.

Fig. 7a shows the crack initiation site in the specimen having 10 μm alumite layer and failed at 300 MPa with N_f = 26,177. Again, a thick region of the alumite layer is found at the fatigue crack initiation site. From this SEM observation, it is again confirmed that the breakage of the alumite layer plays a role as the crack starter during the fatigue process. Fig. 7b shows the crack initiation site of the specimen failed at 125 MPa and with a very long life of N_f = 9970,98,500. Although the crack initiation site is not very clear, the crack appears to be internal initiation, from the overall morphology of fracture surface.

Fig. 8 shows the presence of many micro-cracks at the notch root of specimens with 10 μm thick alumite layer. It is clear that the depth of the crack in this case is also larger than the depth for the specimen with the alumite layer of 3 μm thick. Accordingly, the micro-cracks behave as crack initiators of the alumite layer even at lower stress levels <188 MPa.

In case of the interior-initiated failure, a number of flat facets were observed around the porous area as shown in Figs. 4b, 5b and 7b, respectively. Initiation mechanism of these facets is not clear at the present stage of this work, and this is an important subject to be resolved in the near future.

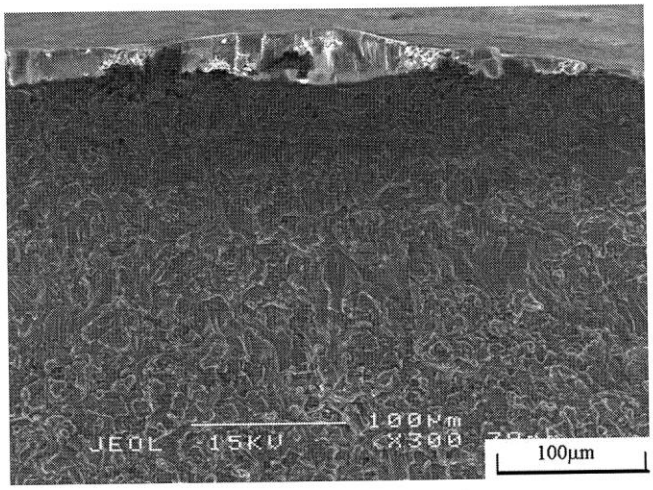

(a) Example at σ_a=300MPa, N_f=26,177

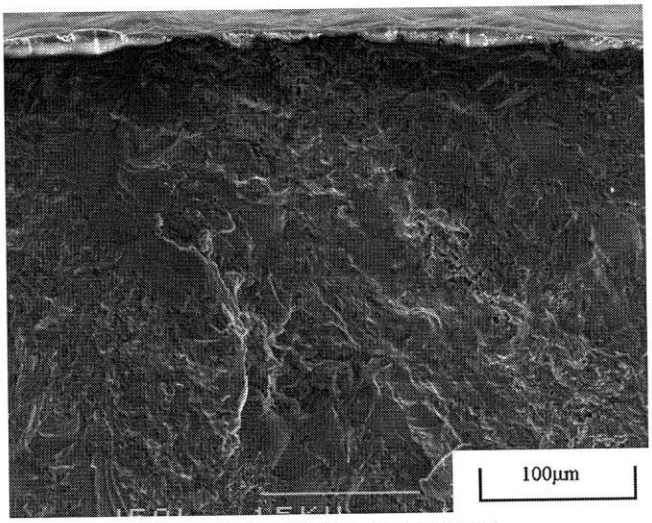

(b) Example at σ_a=125MPa, N_f=997,098,500

Fig. 7. Crack initiation sites in alumite (10 μm) specimens.

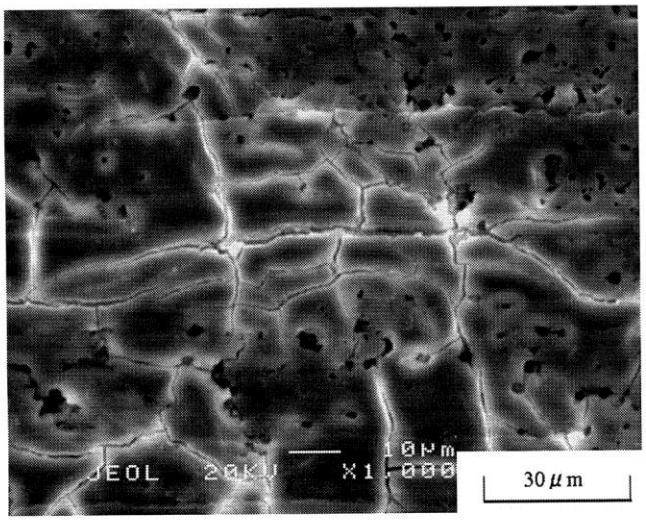

Fig. 8. Presence of micro-cracks at the notch root surface of alumite (10 μm) specimen.

3.3. Fracture mechanics analysis

Micro-cracks are introduced in the alumite layer on the specimen surface during alumite treatment, regardless of the thickness of the alumite layer. In the case of surface-initiated failures in alumite-treated specimens, these micro-cracks seem to propagate into the base-metal and lead to fatigue failure. It can be suggested that the fatigue limit of alumite-treated specimen is governed by the stress below which the micro-crack in the alumite layer can not grow into the base-metal. Based on such a concept, the fatigue limit of the alumite-treated specimen is evaluated quantitatively by applying fracture mechanics, in the following.

The schematics of a surface crack in the alumite layer attempting to propagate into the base-metal are shown in Fig. 9. In the figure, $2a$ is the surface-length and b is the depth of the crack. The depth of the crack is taken to be the thickness of alumite layer. The crack in the alumite layer is approximated by a shallow crack having the shape of a semi-ellipse with the long and short dimensions of a and b, respectively.

Fracture mechanics calculations were performed for: (i) specimens with 3 μm alumite layer and failed at 200 MPa with N_f = 54,800 and (ii) specimens with 10 μm alumite layer and failed at 125 MPa with N_f = 330,581. These two conditions were selected since they correspond to the fatigue limits for alumite-treated specimens having each thickness of the alumite layer in the case of surface-initiated failures.

The ΔK values at the crack tip were calculated by using the following expressions [23];

$$\Delta K = \sigma_a \sqrt{\pi b} F^B_{I,3} \tag{1}$$

$$K^B_{I,2} = \sigma_a \sqrt{\pi b} F^B_{I,2}, \quad \lambda = \frac{a}{d} \tag{2}$$

$$F^B_{I,2} = 1.121 - 1.199\lambda + 4.775\lambda^2 - 1.628\lambda^3 + 7.035\lambda^4 + 13.27\lambda^5 \tag{3}$$

$$K^T_{I,2} = \sigma_a \sqrt{\pi b} F^T_{I,2}, \quad \lambda = \frac{a}{d} \tag{4}$$

$$F^T_{I,2} = 1.12 - 0.231\lambda + 10.55\lambda^2 - 21.72\lambda^3 + 30.39\lambda^4 \tag{5}$$

$$K^T_{I,3} = \sigma_a \sqrt{\pi b} F^T_{I,3}, \quad \lambda = \frac{a}{d}, \quad \beta \frac{b}{a} \tag{6}$$

$$F^T_{I,3} = (1.122 - 0.230\beta - 0.901\beta^2 + 0.949\beta^3 - 0.280\beta^4) \times (1.0 + 0.157\lambda - 0.634\lambda^2 + 4.590\lambda^3 - 6.628\lambda^4) \tag{7}$$

$$F^B_{I,3} = F^T_{I,3} \frac{F^B_{I,2}}{F^T_{I,2}} \tag{8}$$

ΔK values thus calculated give the maximum range of K at the crack tip of the deepest portion of the shallow surface crack in Fig. 9. The ΔK values calculated by varying the aspect ratio, a/b, and for fixed crack depths of 3 μm and 10 μm are plotted in Fig. 10. The ΔK values increase with an increase in a/b, but they become nearly constant at $a/b > 7$. This fact suggests that the very long shallow cracks in the alumite layer can be well approximated by a semi-ellipse crack having the aspect ratio of $a/b \cong 7$ or greater. The asymptotic values of ΔK are 1.30 MPa$\sqrt{m}$, and 1.38 MPa$\sqrt{m}$, respectively for 3 μm and 10 μm alumite layers. These values are nearly the same and it can be said that the fatigue limit of alumite-treated specimens in the surface-initiated failure is governed by a critical ΔK value of about 1.3–1.4 MPa$\sqrt{m}$ for crack penetration into the substrate metal.

As another useful evaluation of small defects, Murakami et al. had proposed the following formula [24];

$$\Delta K = \alpha \Delta \sigma \sqrt{\pi \sqrt{area}} \tag{9}$$

where α = 0.65 for surface crack. Typical crack length is supposed to be 80 μm for specimens with 3 μm alumite layer in Fig. 6, whereas

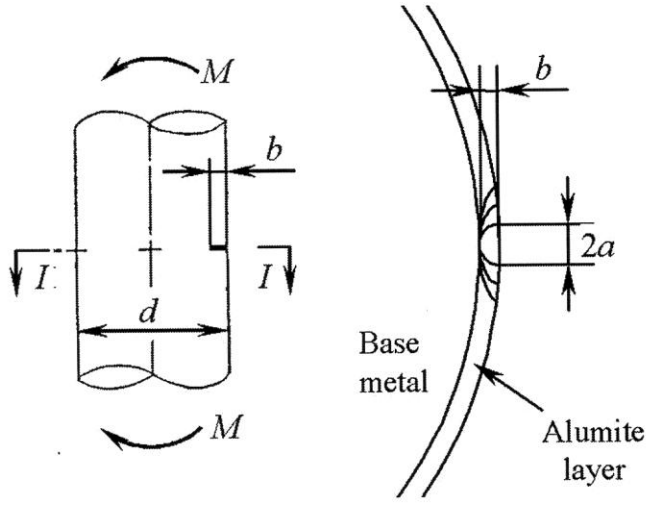

Fig. 9. Schematic illustration of specimen having surface crack.

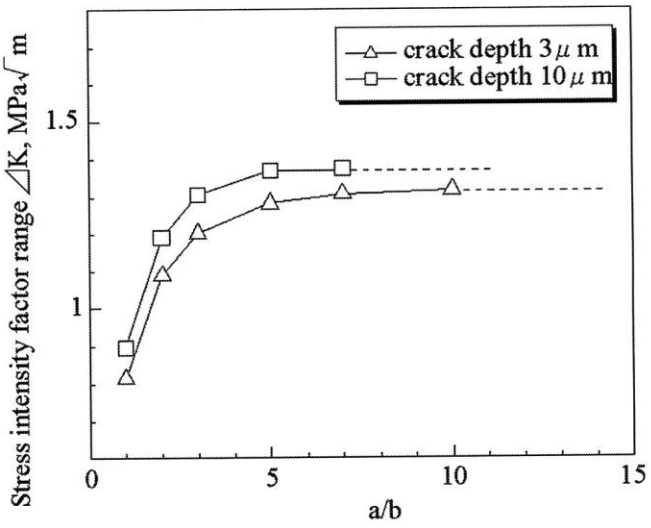

Fig. 10. Relationship between ΔK and a/b.

the crack length is about 120 μm for specimens with 10 μm alumite layer in Fig. 8. By substituting the respective data into Eq. (9), we obtain the values of ΔK as follows:

- 0.91 MPa $\sqrt{m}$ for 3 μm alumite layer at $\Delta\sigma$ = 200 MPa;
- 0.85 MPa $\sqrt{m}$ for 10 μm alumite layer at $\Delta\sigma$ = 125 MPa.

These values are very close to each other, although they are a little smaller than those calculated by Eqs. (1)–(8). Threshold value of ΔK_{th} for a cast aluminum alloy (W319-T6) is reported to be in the range of 0.8–1.0 MPa$\sqrt{m}$ under the same stress ratio of $R = -1$ [25]. Values calculated by Eq. (9) are in excellent agreement with the values in Ref. [25].

Based on the above evidence, it is finally found that the interior-initiated failure takes place at low stress levels giving ΔK values less than the critical level required to the propagation of micro-cracks in the alumite layer into the parent material. In such a case, the alumite layer can carry the load to some extent and, therefore, the stress on the parent material becomes a little lower than that of the untreated specimen. This is a reason why the fatigue life of specimens coated by 3 μm alumite is longer than that of untreated specimens.

The above calculation of ΔK was performed under the assumption that the bending load was applied to a round bar having a shallow surface crack. Difference of material properties of the alumite layer and the parent material is not taken into account in the present analysis. Thus, the above calculation provides only the apparent analysis of ΔK by assuming homogeneous material for the sake of reference. It is noted that the analytical results thus obtained are in good agreement with the experimental results reported by other researchers [26,27].

4. Conclusions

(1) For aluminum alloy specimens of TF12B without alumite treatment, the surface-initiated failure took place at stress levels ≧175 MPa, whereas the interior-initiated failure occurred at stress levels <175 MPa. However, *S–N* curves for the respective failure modes were still smoothly connected at the critical stress level ≅175 MPa such that we have a smooth *S–N* curve in a wide cycle range of $10^3 < N < 10^9$.

(2) For alumite-treated specimens having 3 μm alumite layer, the failure mode shifted from surface-initiated failures to interior-initiated failures at the stress level of about 188 MPa. Thus we have the duplex *S–N* characteristics indicating a significant step at the critical stress level of about 188 MPa. At stress levels ≧188 MPa, fatigue life of the alumite-treated specimen is lower than that of the untreated specimen. But, at stress levels <188 MPa, fatigue life of this kind of specimen becomes higher than that of the untreated specimen.

(3) For specimens having 10 μm alumite layer, a significant deterioration of the fatigue strength is observed in comparison with the results for all other surface conditions. The *S–N* characteristics of the specimen with 10 μm alumite layer appear to have the clear fatigue limit ≅119 MPa, as often observed in ferrous metals.

(4) In the case of surface-initiated failure in alumite-treated specimens, origin of the dominant fatigue crack leading to the final failure corresponded to the thickest site in the alumite layer. Interior-crack-initiations were caused by clusters of pores.

(5) Very long shallow cracks can be well approximated by a semi-ellipse crack having the aspect ratio of $a/b \cong 7$. Based on the quantitative analysis of stress intensity factor range at the crack tip of alumite layer, it is found that the surface-crack-fatigue-limit of alumite-treated specimen is governed by a critical ΔK_{th} value of about 0.8–1.4 MPa$\sqrt{m}$ for crack penetration into the substrate metal.

References

[1] Bathias C, Paris PC. Gigacycle fatigue in mechanical practice. New York: Marcel Dekker; 2005. p. 1–7.
[2] Mughrabi H. Zur dauerschwingfestigkeit im bereich extrem hoher bruchlastspielzahlen: Mehrstufige lebensdauerkurven. Haerterei-Tech Mitt 2001;56(5):300–3.
[3] Sakai T, Sato Y, Nagano Y, Takeda M, Oguma N. Effect of stress ratio on fatigue behavior of high carbon chromium steel under axial loading. Int J Fatigue 2006;28(11):1547–54.
[4] Sakai T. Review and prospects for current studies on very high cycle fatigue of metallic materials for machine structural use. In: Proceedings of VHCF-4; 2007. p. 3–12.
[5] Sakai T, Tanaka N, Takeda M, Kanemitsu M, Oguma N. Characteristic *S–N* property of high strength steels in ultra-wide life region under rotating bending. In: Proceedings of EcoDesign; 2001. p. 432–7.
[6] Sakai T, Amano K. Realization of resources saving and reduction of global environmental load based on expansion of design life for industrial products. J Environ Conserv Eng 2008;37(9):39–45.
[7] Bayractar E, Bathias C, Hongquian X, Hao T. On the gigacycle fatigue behaviour of two-phase ($\alpha_2 + \gamma$) TiAl alloy. Int J Fatigue 2004;26(12):1263–75.
[8] Sakai T, Sato Y, Oguma N. Characteristic *S–N* properties of high-carbon–chromium-bearing steel under axial loading in long-life fatigue. Fatigue Fract Eng Mater Struct 2002;25(8/9):765–73.
[9] Stanzl-Tschegg SE. Fracture mechanisms and fracture mechanics at ultrasonic frequencies. Fatigue Fract Eng Mater Struct 1999;22(7):567–79.
[10] Allison JE, Jones JW, Larsen JM, Ritchie RO. Very high cycle fatigue. In: Proceedings of VHCF-4. TMS; 2007.
[11] Sakai T, Ochi Y, Jones JW. In: Foreword: special issue on the 3rd Int Conf on very high cycle fatigue (VHCF-3) held in Kyoto/Kusatsu, Japan, 16–19 September 2004, Int J Fatigue 28(11); 2006. p. 1437.
[12] Bathias C, Miller KJ, Stanzl-Tschegg SE. Editorial: Gigacycle fatigue. Fatigue Fract Eng Mater Struct 1999;22(7):543.
[13] Sakai T, Takeda M, Tanaka N, Kanemitsu M, Oguma N, Shiozawa K. Characteristic *S–N* property of high carbon chromium bearing steel in ultra-wide life region under rotating bending. Mater Sci Res Int STP 2001;1:41–6.
[14] Zhu X, Shyam A, Jones JW, Mayer H, Lasecki JV, Allison JE. Effect of microstructure and temperature on fatigue behavior of E319-T7 cast aluminum alloy in very long life cycles. Int J Fatigue 2006;28(11):1566–71.
[15] Kubota H, Ochi Y, Ishii A, Shibata R. Improvement of high cycle fatigue properties by HIP treatment for cast aluminum alloy. Trans Jpn Soc Mech Eng 1995;61(591):2342–8.
[16] Ochi Y, Hatakeyama A, Matsumura T, Shibata R. High cycle fatigue strength and fatigue crack properties of semi-liquid die casting aluminum alloy. Trans Jpn Soc Mech Eng 2000;66(649):1703–9.
[17] Sakai T, Hirano H, Nishida T, Tomoto T. A study on ultra long life fatigue characteristics in rotating bending for aluminum alloy with some surface treatments. In: Proceedings of VHCF-3; 2004. p. 585–92.
[18] Jono M et al., editors. Handbook on fatigue design, section 1.2. Yokendo; 1995.
[19] Peterson RE. Stress concentration design factors. New York: John Wiley & Sons, Inc; 1953. p. 50.
[20] Sakai T, Takeda M, Shiozawa K, Ochi Y, Nakajima M, Nakamura T, Oguma N. Experimental reconfirmation of characteristic *S–N* property for high carbon chromium bering steel in wide life region in rotating bending. J Soc Mater Sci Jpn 2000;49(7):779–85.
[21] Sakai T, Furusawa T, Takizawa R, Oguma N, Hohjo H, Ikuno H. Development of multi-type high frequency fatigue testing machines in rotating bending and axial loading. In: Proceedings of Hael Mughrabi Honorary symposium, 137th annual meeting and exhibition. TMS2008; 2008. p. 241–6.
[22] Sakai T, Takeda M, Shiozawa K, Ochi Y, Nakajima M, Nakamura T, et al. Experimental evidence of duplex *S–N* characteristics in wide life region for high strength steels. In: Proceedings of 7th international fatigue congress, vol. 1; 1999. p. 573–8.
[23] Edited by the JSMS Committee on fracture mechanics, The Society of Materials Science Japan, Stress intensity factors handbook, vol. 2. Pergamon Press; 1987. p. 657–8.
[24] Murakami Y. Metal fatigue: effects of small defects and nonmetallic inclusions. Yokendo Ltd; 1993. p. 17.
[25] Caton MJ, Jones JW, Allison JE. The influence of heat treatment and solidification time on the behavior of small-fatigue-cracks in a cast aluminum alloy. Mater Sci Eng A 2001;314(1-2):81–5.
[26] Couper MJ, Neeson AE, Griffiths JR. Casting defects and the fatigue behaviour of an aluminium casting alloy. Fatigue Fract Eng Mater Struct 1990;13(3):213–27.
[27] McDowell DL, Gall K, Horstemeyer MF, Fan J. Microstructure-based fatigue modeling of cast A356-T6 alloy. Eng Fract Mech 2003;70:49–80.